August 1989

BNL- 43250

CONF-8908165--1

THE USES OF SYNCHROTRON RADIATION SOURCES FOR ELEMENTAL AND CHEMICAL MICROANALYSIS

BNL--43250

DE90 001269

J. R. Chen, E. C. T. Chao, J. A. Minkin, J. M. Back,

K. W. Jones, M. L. Rivers, and S. R. Sutton

Invited Paper Presented at

5th International Conference on PIXE and Its Analytical Appplications

Amsterdam, The Netherlands

August 20-26, 1989

THE USES OF SYNCHROTRON RADIATION SOURCES FOR ELEMENTAL AND CHEMICAL MICROANALYSIS

J.R. Chen[1)], E.C.T. Chao[2)], J.A. Minkin[2)], J.M. Back[2)], K.W. Jones[3)], M.L. Rivers[3)], and S.R. Sutton[3)]

[1)]State University of New York, Geneseo, NY 14454, USA
[2)]US Geological Survey, Reston, VA 22092, USA
[3)]Brookhaven National Laboratory, Upton, NY 11973, USA

ABSTRACT

Synchrotron radiation sources offer important features for the analysis of a material. Among these features is the ability to determine both the elemental composition of the material and the chemical state of its elements. For microscopic analysis synchrotron x-ray fluorescence (SXRF) microprobes now offer spatial resolutions of 10μm with minimum detection limits in the 1-10 ppm range depending on the nature of the sample and the synchrotron source used.

This paper describes the properties of synchrotron radiation and their importance for elemental analysis, existing synchrotron facilities and those under construction that are optimum for SXRF microanalysis, and a number of applications including the high energy excitation of the K lines of heavy elements, microtomography, and XANES and EXAFS spectroscopies.

DISCLAIMER

Invited paper for the 5th International Conference on PIXE and Its Analytical Applications, Vrije University, Amsterdam, The Netherlands, August 20-26, 1989.

1. Introduction

The availability of dedicated synchrotron radiation sources offers some unique capabilities for the characterization of a material. Elemental identification as well as chemical and structural information can be obtained. For microscopic analysis SXRF microprobes now offer spatial resolutions of 10μm with minimum detection limits (MDLs) in the 1-10 ppm range depending on the material being analyzed and the synchrotron source used. Lower spatial resolutions (0.1-1μm), comparable to that of electron probe microanalysis (EPMA) and particle induced x-ray emission (PIXE), with MDLs in the 10-100 ppb range are projected for synchrotron sources currently under construction. In addition, for applications dealing with delicate samples, e.g., polymers and biological specimens, where radiation damage has been an important concern, SXRF microprobes deposit several orders of magnitude less energy in the sample for the same MDL when compared with EPMA or PIXE microprobes [1,2]. SXRF analyses are usually carried out in air or helium, and not in a vacuum as is often the case with other techniques. Thus live or wet biological specimens can be readily studied using SXRF.

This paper provides an overview of the current and future applications of synchrotron radiation microanalysis. Section 2 describes the production and properties of synchrotron radiation from storage ring bending magnets and insertion devices such as wigglers and undulators. Synchrotron radiation facilities that are optimum for SXRF are characterized by their production of hard x-rays, which are capable of exciting the K lines of all elements in the periodic table, and by their high brilliances (10^{15}-10^{18} photons/s/mm^2 source area/mrad^2/0.1% bandwidth). SXRF microprobes that have been recently constructed or are under construction are the subject of section 3. Finally, representative applications of synchrotron radiation microanalysis to (1) the heavy element characterization of geological samples using K line excitation, (2) microtomography, and (3) the

determination of the chemical state and molecular structure of an element, are the subjects of section 4.

2. Production of synchrotron radiation

Whenever electrically charged particles are accelerated, they emit electromagnetic radiation. Examples of this phenomenon include the scattering of electrons by the electric field of a nucleus which produces bremsstrahlung, and the acceleration of electrons constrained by a magnetic device (e.g. bending magnets, wigglers, undulators) in a storage ring accelerator, which produces synchrotron radiation.

Radiation from bending magnets:

An observer in the laboratory looking along the tangent to the curved orbit of an electron or positron in a bending magnet would receive a pulse of synchrotron radiation each time the electron passed by. This pulse can be Fourier-analyzed to give a continuous energy spectrum.

The average integrated power of the radiation is given by [3]:

$$P\ (kW) = 0.633\ E^2 I \int B^2 dz$$

where I(amp) is the average electron current circulating in the storage ring and $\int B^2 dz$ is taken over the portion of the trajectory seen by the observer. High integrated power results from high values of the electron energy E(GeV), large magnetic fields B(Tesla), and the use of multipole wigglers and undulators in the straight sections of the storage ring.

Synchrotron radiation is naturally collimated in the vertical direction with an opening angle given by:

$$\theta_v \simeq \frac{1}{\gamma} = \frac{mc^2}{E}$$

For typical electron energies E = 2.5-7 GeV, θ_v is 70-200 μrad. The radiation is therefore produced as a "very thin" horizontal sheet. For an observer at $\theta_v = 0$, the radiation is linearly polarized with the electric field vector in

the electron orbital plane. For SXRF this high linear polarization is useful in reducing the Raleigh and Compton scattered background under the fluorescence signal.

The spectral brilliance of bending magnet radiation at the National Synchrotron Light Source (NSLS), and a facility under construction, the Advanced Photon Source (APS), are shown in figure 1. It is currently feasible to produce a 10 keV microbeam at the NSLS with intensities of 3×10^7 photons/s/μm^2 in a $\approx$ 10μm beam spot with a $\Delta E/E = 0.1$ and obtain 1-40 ppm MDLs for elements from K to Zn in 1 mg/cm^2 samples in 60 s run times [4]. Calculations indicate that an increase in the intensity by two orders of magnitude is feasible.

Radiation from wigglers and undulators:

A wiggler or undulator is a device with a periodic magnetic structure. Such a device can be inserted in a straight section of a storage ring without altering the electron's orbit in the rest of the ring, if the integral of the field along the orbit coordinate is zero. For the case where the B field varies sinusoidally with period λ_o(cm) and is in the vertical direction:

$$B(z) = B_o \sin\left(\frac{2\pi z}{\lambda_o}\right),$$

the electron motion is also sinusoidal and lies in the horizontal plane (figure 2). The angle of deflection δ is given by:

$$\delta = \frac{0.3}{E} \int B(z)dz = \frac{K}{\gamma} \cos\left(\frac{2\pi z}{\lambda_o}\right)$$

where $K = 0.934 B_o \lambda_o$. In terms of K, the maximum angle of deflection of the orbit is $\delta_{max} = K/\gamma$. If $K > 10$, then $\delta_{max} > 1/\gamma$ and the device is called a wiggler. If $K < 1$ (e.g. moderate B fields and possibly a large number of poles), then $\delta_{max} < 1/\gamma$ and the device is called an undulator. Insertion devices with $1<K<10$ produce features that are intermediate between those of wigglers and undulators.

For a wiggler large deflections of the electrons occur. For an APS wiggler

A the horizontal opening angle of the radiation is about ± 1 mrad. The large opening angle contributes to the smaller brilliance than that from undulators, but the wiggler spectrum extends to energies in excess of 100 keV (figure 1). The emission in any direction is given approximately by the incoherent sum of the emissions from the points of the trajectory to which the direction of observation is tangent. The spectrum is, therefore, to a good approximation equal to that from a bending magnet of the same magnetic field, scaled by the number of poles in the wiggler.

For an undulator synchrotron emissions from the entire length of the trajectory in the undulator are collected and strong interference effects are observed. The photons are concentrated into quasi-monochromatic ($\Delta E/E \approx 1\%$) bands. The undulator radiation is highly collimated in both the horizontal and vertical directions; the characteristic opening angle is approximately 10-25 μrad for an APS undulator A, which is less than the 70μrad intrinsic vertical opening angle of the bending magnet radiation. Figure 1 depicts the brilliance expected from an undulator A at the APS. With brilliances approaching 10^{18} photons/s/mm^2/mrad^2/0.1% bw at 10 keV, assuming a 200:1 demagnification of the source size ($4\ \sigma_x = 1.2$ mm, $4\ \sigma_y = 0.3$ mm, $\sigma'_x = 24$ μrad, $\sigma'_y = 9$μrad) and a 25% collection efficiency, intensities will be about 2×10^{12} photons/s/μm^2 in a 3μm spot with a $\Delta E/E = 1 \times 10^{-3}$. This is over 4 orders of magnitude greater than the intensity feasible from the NSLS bending magnet microprobe. In principle we will then have the important choice of decreasing the beam spot to below 0.1 μm for intensities similar to those at the NSLS, decreasing the MDLs to the 8-300 ppb level, or using an advantageous combination of beam size and MDLs depending on the experiment. This assumes that suitable optics can be fabricated to produce such small beam spots, and detectors capable of handling the increased count rate associated with the above MDLs can be built. Some lowering of the MDLs over current levels can be expected because the undulator radiation is quasi-

monochromatic. In addition to the high brilliance of an undulator, the energy of the photons produced can be tuned by changing the gap of the undulator. For example, the APS undulator A will deliver radiation from 4-14 keV in the fundamental and from 12-40 keV in the third harmonic by varying the gap from 1.0 to about 2.8 cm. This tunable quasi-monochromatic undulator radiation is particularly valuable for experiments where the incident energy must be tuned through an absorption edge.

Over the last few years there has been a major effort to harden the synchrotron radiation by increasing the storage ring energy and using wigglers, and to increase the brilliance by reducing the source emittance (the product of the electron beam size and divergence) and using undulators. SXRF has benefited from these developments. It is currently feasible to excite the K lines of the rare earth elements because of the hardened spectrum. Current dedicated sources operate with horizontal beam emittances in the 100 nm rad range. Future facilities promise significant improvements [5-7]. The APS and the European Synchrotron Radiation Facility (ESRF), both of which are expected to be completed in the 1990's, will have horizontal emittances less than 10 nm rad.

For comparison figure 1 also shows the brilliance from conventional x-ray tubes, which are 10^4-10^8 times less brilliant.

3. Synchrotron x-ray fluorescence microprobe

The high brilliance and natural collimation in the vertical direction characteristic of synchrotron radiation are favorable factors for the construction of microprobe beams. Table 1 lists the SXRF microprobes that have been recently constructed or are under construction. The synchrotron radiation is either collimated or focused using shaped mirrors or crystals to produce a 10-50μm beam spot. The sample is positioned in the beam by (x,y,z,θ) motor-driven stages, because the beam cannot be moved electrostatically or magnetically as with charged particles. The fluorescent x-rays and scattered beam are detected with an energy-

dispersive spectrometer (EDS) and/or a wavelength-dispersive spectrometer (WDS).

Collimated white microbeams:

The simplest approach to defining a microbeam uses a pinhole collimator. Filters may be used to crudely shape the energy spectrum of the white beam. Despite the significant loss in intensity inherent to collimation, a sufficiently large number of photons are left in a typical 30μm pinhole to carry out SXRF measurements. At DORIS a 50μm beam was used to study aerosol samples with 1.5 ppm MDLs [8]. Spatial resolutions down to 3μm were obtained using a line scanning technique [9]. At VEPP-3 Baryshev et al. [10] have studied rock samples using a 30μm beam. The most extensive use of collimated beams has been made at the NSLS where a 30μm beam with 1 x 10^{10} photons/s ($\Delta E/E \approx 1$) has been used in a variety of studies in biology, cosmochemistry and the earth sciences [11-19].

Collimated monochromatic microbeams:

In order to optimize the MDL for a particular element, a monochromatic beam with an energy just above the absorption edge of the element is required. The sharp rise in the photoelectric cross section at an absorption edge accounts in part for the attractiveness of the SXRF technique for element identification. Attempts to monochromatize the collimated beam have been reported by Baryshev et al. [10] at VEPP-3. A flat pyrolytic graphite crystal was used to produce energies from 8-35 keV; 10 ppm MDLs for elements from Fe to Sr were achieved in 1 to 3 s runs. At the Photon Factory a flat Si(111) crystal was used as a monochromator, and collimation in one dimension produced beam spots <40μm (H) x 3 mm (V) [20]. A beam energy of 12.6 keV was chosen to excite As and Ga K x-rays in a contamination layer formed on an InP substrate. Figure 3 shows two sample arrangements: (1) at 45° the As and Ga concentrations can be determined with MDLs of 2 x 10^{13} atoms/cm^2, and (2) at 1-6 mrad grazing incidence angles the concentrations can be determined with an order of magnitude lower MDLs and, in addition, a depth profile analysis can be made. Total x-ray reflection occurs

for angles below a critical angle of 3.3 mrad. Since the penetration depth of the incident x-rays varies from a few tens of Å to a few μm around the critical angle, a depth distribution of an element can be derived from the angular dependence. Under total reflection conditions the shallow penetration of the incident beam also leads to a reduction in the scattered radiation and to reduced In Lα counts from the substrate. Iida et al. [21] have reported MDLs <1 ppb in solution in 100 s counting times for aqueous solutions of Zn, Mn, and Ca dried on Si reflectors.

Focused microbeams:

The usefulness of a SXRF microprobe is greatly enhanced if the high brilliance of the source, which is partially wasted in a collimated microprobe, can be utilized by means of focusing elements. Two optical elements are available: mirror surfaces that redirect the beam by total reflection, and crystals and multilayer microstructures that redirect the beam by Bragg scattering.

Two considerations are borne in mind in designing a SXRF microprobe: (1) To intercept a given divergence of synchrotron radiation, mirrors must have larger physical dimensions than crystals and multilayer structures. This results from the fact that the angle of incidence for total reflection of up to 20 keV photons, for example, is typically 4 mrad for a Pt-coated mirror, while the Bragg angle is 100 mrad for crystal diffraction from Si and 8 mrad for a multilayer structure with a d-spacing of 40 Å. The production of large x-ray mirrors tests the state of the art technology; and (2) crystals and multilayer structures monochromatize the beam as well. A separate monochromator must be used with a focusing critical reflection mirror. The separation of the focusing and monochromatizing functions is an advantage for experiments that require a focused white beam for multielement analysis and can tolerate lower signal to background ratios. In such experiments the monochromator is retracted from the beamline.

Focusing with monochromatization:

Figure 4a shows the microprobe design at the SRS [22]. The focusing element is a circular doubly bent (toroidal) Si(111) crystal. With fixed radii of curvature, the focus is optimized for one energy at 20 keV and the bandwidth is $\Delta E/E = 2.5 \times 10^{-2}$. About 2×10^7 photons/s are produced in a 30μm spot for 100 mA current in the storage ring. Recent additions include an ellipsoidal crystal. With the completion of the high brightness lattice at the SRS, higher intensities can be expected.

Figure 4b shows a schematic of the microprobe developed at the Lawrence Berkeley Laboratory [4]. For grazing incidence, because the sagittal rays of a given spherical mirror are weakly focused compared to the tangential rays and an astigmatic focus therefore results, the mirrors are arranged in a Kirkpatrick-Baez configuration. In this configuration the sagittal rays of the first mirror become the tangential rays for the second mirror (and vice versa), and are strongly focused to reduce the astigmatism. The mirrors are coated with alternating layers of two elemental materials of very different atomic numbers (e.g. W and C). These layers form a microstructure of periodically varying electron density, which diffracts x-rays much like a crystal. The reflectivity of the mirror varies with incident angle θ, and reaches a maximum at angles given by the Bragg relation

$$n\lambda = 2d_1 \sin\theta_1 = 2d_2 \sin\theta_2.$$

By controlling the thickness of the layer pair, the energy and output angle can be selected. With the fixed mirror system (both mirrors have a 2 cm diameter, radius of curvature of 6 m and surface roughness <3 Å; $d_1 = 29$ Å and $d_2 = 44$ Å), the microprobe delivers a fixed energy of 10 keV at the focus. The bandpass is large, i.e. $\Delta E/E = 1 \times 10^{-1}$. A beam spot of ≈ 10μm with an intensity of 3×10^7 photons/s/μm² has been achieved and used in a series of experiments [23]. A similar microprobe designed to focus 17 keV photons is currently being tested.

Focusing without monochromatization:

Spherical mirrors do not yield perfect point to point focusing. In fact, with the geometry shown in figure 4b, a point source produces a 25μm distance between the extreme rays at the image. The ideal geometry for focusing a point source is an ellipsoid. Even for an extended synchrotron source, an ellipsoid surface is the best configuration to achieve a small focus.

At the Photon Factory two Wolter type 1 optical systems are used to achieve a beam spot <10μm (V) x 30μm (H) with energies up to 10 keV (figure 4c) [24]. At the NSLS the SXRF microprobe shown schematically in figure 4d is currently being installed [25]. The overall design concept is to monochromatize the beam with a Si channel-cut crystal. This avoids contributions to the angular divergence from factors such as mosaic spreads, which are characteristic of microcrystalline materials like graphite. The beam is then focused with an ellipsoidal mirror. The separation of the monochromatizing and focusing functions allows for a system simpler to construct. Focusing a monochromatic beam eases the power stress on the system optics. Further, the monochromator will be fully retractable from the beamline in order to allow for a focused white beam required by some experiments. In the initial design specifications the 8:1 ellipsoidal mirror is a grazing-incidence, totally reflecting, Pt-coated (onto Al substrate) mirror with a minor radius of 28.3 mm and a major radius of 9000 mm [26]. At an angle of incidence of 5 mrad, energies up to 17 keV will be focused. To accept most of the vertical angular divergence (0.2 mrad) of the synchrotron beam, the length of the mirror at 8 m must be 30 cm. The mirror is designed to accept 0.5 mrad in the horizontal direction. Reduction of the NSLS source size of 0.5 mm (V) x 1.5 mm (H) by a factor of 8 gives an image of 63μm minimum dimension. The beam spot is then defined with a 5-30μm pinhole collimator a few mm upstream of the target. For 100 mA storage ring current, projected intensities are 4 x 10^{11} photons/s at 15 keV, about 3 orders of magnitude higher than

the intensity from a collimated beam.

4. Representative applications of synchrotron radiation microanalysis

To date there have not been many published applications of synchrotron radiation microanalyses using focused beams. By far the largest number of actual applications has been with collimated beams. For example, at the NSLS an intensity (from a bending magnet source) of 1×10^{10} photons/s in a 30μm collimated spot has been used in a variety of biological, chemical, and geological applications.

To illustrate the broad unique applicability of synchrotron radiation microanalysis, in addition to the depth profile analysis mentioned in section 3, a number of selected examples are cited below.

High energy excitation of the K lines of the rare earth elements [27,28]:

The study of the concentrations and distributions of the rare earth elements (REEs) in specific mineral grains by fluorescence analysis can be accomplished by excitation of the REE L lines between 4.6 and 10.1 keV, or their K lines between 33.0 and 62.9 keV. Both PIXE and SXRF can be used to excite the L lines. However, because of the numerous mutually overlapping Lα, Lβ, Lγ, etc. lines within the narrow 5.5 keV span, sophisticated computer programs are required to deconvolute the spectra. In addition, the K lines of Ti, Fe, Co, Ni, Cu, Zn, Ga, and Ge lie within the indicated energy range, which makes the analysis difficult for some minerals even with a wavelength-dispersive spectrometer.

Excitation of the REE K lines using 40 MeV protons [29] and high energy synchrotron beams is practical; and due to the large 29.9 keV span, Si(Li) and Ge(Li) multielement detectors with 0.4 keV resolution can be used to resolve the lines.

The Bayan Obo ore deposit, located in Inner Mongolia, China, is recognized as the world's largest REE deposit with an estimated reserve of 35×10^6 metric

tons of REE oxide. REEs are now recognized as strategic resources; it is important to understand the origin and mode of occurrence of this deposit in order to explore for similar deposits. Site-specific data on single mineral grains are needed to address questions of the REE sources, their epigenetic hydrothermal-metasomatic versus igneous or metamorphic orgin, and their possible remobilization [31].

A preliminary study of REE-rich Bayan Obo minerals was carried out at the NSLS using high energy SXRF microprobe analysis [30]. Ta absorbers were used to attenuate the low energy (<30 keV) synchrotron photons, which were incapable of exciting the K lines of the REEs. This greatly reduced the sample scattering of the continuum radiation which is the dominant background under the fluorescence peaks for white radiation excitation.

The samples were prepared as 30μm thick doubly polished thin sections on a thin supporting substrate (500μm thick pure silica glass discs). This sample thickness facilitated petrographic analysis in transmitted and reflected light prior to SXRF microanalysis. Individually selected mineral grains and standard materials were also mounted in epoxy on the glass discs. Figure 5 shows the SXRF spectrum from an aeschynite mineral grain. MDLs in the 100 ppm range for 3600 s counting times using a 40μm beam spot were obtained.

At 60 keV the brightness from an APS bending magnet is expected to be 5 x 10^3 times that of a NSLS bending magnet. Thus it should be possible to reduce the beam spot to 10μm and detect 5 ppm of the REEs at the APS. At 60 keV the brightness from a wiggler at APS is more than 5 orders of magnitude greater than that of a NSLS bending magnet. With such a wiggler the spot size should be reducible to below 1μm with MDLs for the REEs in the 1-5 ppm range using K lines. Alternately, one could use a monochromatic beam to selectively excite a given REE and/or use a WDS to improve the signal to background ratio.

Computerized microtomography:

In computerized tomography (CT) it is possible to obtain an image of a thin cross section of a 3-dimensional object. Conventional x-ray tubes, however, limit the image resolution to a few mm and, when the object is human, the continuous energy spectrum emitted by the x-ray tubes limit the dosage that can be tolerated. Monochromatic synchrotron radiation can be tailored to excite a specific element of interest and results in less energy deposition in the object. If the full intensity of a synchrotron beam is not a problem e.g. with biopsy samples, industrial materials, etc., image resolutions of 1-5μm are feasible.

At the NSLS an ant head was irradiated with a 10μm (V) x 17μm (H) collimated synchrotron beam and the transmitted beam detected with an Ar proportional counter [19]. After every 0.08 s, the sample was translated horizontally by 17μm until a distance of 3.6 mm was irradiated. (Continuous scanning was also used for some runs.) The sample was then rotated about a vertical axis by a small angle and the above irradiation procedure repeated. After 276 such rotations totalling 180° and lasting 82 minutes, the reconstructed image shown in figure 6 was obtained. This image represents a 10μm thick horizontal slice through the ant head with a spatial resolution of 17μm.

For rapid imaging Suzuki et al. [32] have used a CT set-up at the Photon Factory, which employs a vertically-collimated horizontally-fan-shaped beam and a 1-dimensional horizontal detector array to detect the transmitted beam. A monochromatic beam allowed superior contrast by using the difference between two images just above and below the absorption edge of a given element. A reconstructed image could be obtained in 15 minutes. Three-dimensional maps of small samples scanned in <1 h with resolutions of 2.5μm have been reported by Flannery et al. [33]. The CT system consisted of a high resolution x-ray detector that recorded data simultaneously in two dimensions. After rotating the sample a 3-

dimensional image could be reconstructed using high speed computer algorithms. At the heart of the system is a cellular phosphor detector that converted the transmitted x-rays to optical radiation. Once converted to optical light, the image was magnified with a conventional lens system and focused onto a solid state charge-coupled detector (CCD). The resolution was determined by the spacing of the phosphor cells.

XANES and EXAFS applications:

While EPMA, PIXE and conventional SXRF microanalysis discussed above are independent of the chemical state of the elements under study, such information is often vital, for example, in understanding the metabolism of toxic trace elements and metals in metalloproteins. One of the most attractive applications of synchrotron radiation is the development of x-ray absorption near edge structure (XANES) and extended x-ray absorption fine structure (EXAFS) analyses, by which the chemical state and coordination (number, type, distances from neighbors) of an individual element in a material can be determined at dilute (100 ppm to 1%) concentrations.

XANES and EXAFS refer to the small variations or fine structure in the absorption coefficient of a material as the energy of the incident synchrotron beam is varied from approximately 100 eV below to 1000 eV above the K absorption edge of a specific element in the material. Figure 7 shows a schematic of the x-ray absorption cross section near a K edge [34]. The region from 20 eV below to approximately 50 eV above the absorption edge is called the XANES region. In this region, the 1s electron is excited to unoccupied higher energy levels. Shifts in the value of the absorption edge energy occur, depending on the amount of shielding from the nucleus that the K shell electron experiences, which in turn depends on the chemical state of the absorbing atom. For higher incident energies, the kinetic energy imparted to the 1s electron is sufficiently large that the electron leaves the atom and may be backscattered from nearby atoms.

The resulting interference between the outgoing and backscattered waves gives rise to the characteristic EXAFS modulation from approximately 50 to 1000 eV above the absorption edge. The Fourier-analyzed EXAFS data yield structural information on the coordination of nearby atoms. EXAFS modulations are observed in absorption, fluorescence, Auger, photoelectron emission and other phenomena.

In its simplest form XANES provides chemical state information as follows: the line shape and position of the absorption edge of a particular element are determined by monitoring the ratio of transmitted to incident beam (absorption mode) (or the fluorescence intensity in the emission mode) as the energy of the incident synchrotron beam is varied; the results are then compared with those of model compounds covering the range of chemical states of the element in question. A high resolution monochromatic beam, such as those from Bragg diffracting crystals with $\Delta E/E = 1 \times 10^{-4}$, is required. Figure 8 shows the absorption spectrum of Co metal, CoO and Co_3O_4 at 0.4 eV intervals as adapted from Sakurai et al. [35]. The positions of the absorption edges of the different chemical states of Co are different. These spectra were used to show that magnetic films of Co-O are a mixture of Co and CoO with no admixture of Co_3O_4. Detailed bonding and structural information has been obtained for a wide variety of materials including silicates and oxides [36], silicate melts and quenched glasses [37], and coals [38].

5. Summary

The unique properties of synchrotron radiation offer many features that are useful for the microcharacterization of materials. With the advent of dedicated synchrotron radiation sources such as the NSLS, the Photon Factory, and the SRS, the full development of synchrotron radiation microprobes is underway. The future APS and ESRF sources will provide extremely high brilliances that will allow synchrotron radiation microprobes to rival the most advanced electron probes [39]. To date most of the actual applications of

synchrotron radiation microprobes have been done with collimated beams, but the use of focused monochromatic beams is beginning to emerge [40]. When compared with charged particle excitation, unique applications of synchrotron radiation microanalysis include the efficient excitation of the K lines of the heavy elements, microtomography, and the determination of the chemical state and molecular structure of an element using XANES and EXAFS analyses. The extremely high brilliance of the synchrotron sources under construction will permit SXRF microanalysis of materials at spatial resolutions approaching 0.1-1μm and with MDLs in the 10-100 ppb range.

Acknowledgements

This work was supported in part by the State University of New York, the U.S. Geological Survey, the National Science Foundation (grant EAR-8313683) and the U.S. Department of Energy, Division of Chemical Sciences (contract no. DE-AC02-76CH00016).

References

[1] C.J. Sparks, in: Synchrotron Radiation Research, eds., H. Winick and S. Doniach (Plenum Press, NY, 1980) 459.

[2] D.N. Slatkin, A.L. Hanson, K.W. Jones, H.W. Kraner, J.B. Warren and G.C. Finkel, Nucl. Instr. Meth. 227 (1984) 378.

[3] H. Winick, in: Synchrotron Radiation Research, eds., H. Winick and S. Doniach (Plenum Press, NY, 1980) 11.

[4] J.H. Underwood, A.C. Thompson, Y. Wu and R.D. Giauque, Nucl. Instr. Meth. A266 (1988) 296.

[5] J.V. Smith and M. Manghnani (co-chairs), Workshop Report ANL/APS-TM-3, Argonne Natl. Lab., Argonne, IL (1988).

[6] G.K. Shenoy, P.J. Viccaro and D.M. Mills, Report ANL-88-9 (1988).

[7] ESRF, Foundation Phase Report (1987).

[8] W. Petersen, P. Ketelsen, A. Knoechel and R. Pausch, Nucl. Instr. Meth. A246 (1986) 731.

[9] M. Bavdaz, A. Knoechel, P. Ketelsen, W. Petersen, N. Gurker, M.H. Salehi and T. Dietrich, Nucl. Instr. Meth. A266 (1988) 308.

[10] V.B. Baryshev, N.G. Gavrilov, A.V. Daryin, K.W. Zolotarev, G.N. Kulipanov, N.A. Mezentsev and Ya.V. Terekhov, submitted to Rev. Sci. Instr.

[11] J.R. Chen, E.C.T. Chao, J.A. Minkin, J.M. Back, W.C. Bagby, M.L. Rivers, S.R. Sutton, B.M. Gordon, A.L. Hanson and K.W. Jones, Nucl. Instr. Meth. B22 (1987) 394.

[12] E.C.T. Chao, J.R. Chen, J.A. Minkin and J.M. Back, Process Mineralogy VII, TMS/AIME, eds., A.H. Vassilou, D.M. Hansen and D.J.T. Carbon (Metallurgical Soc., Inc., Warrendale, PA, 1988) 143.

[13] R.N. White, D.A. Spears and J.V. Smith, (abstract) GSA meeting (1988).

[14] D.R. Baker and E.B. Watson, Proc. 9th Univ. Conf. on Glass (Rensselaer Polytechnic Institute, NY, 1987).

[15] S.R. Sutton, J. Delaney, J.V. Smith and M. Prinz, Geochim. Cosmochim. Acta 51 (1987) 2653.

[16] S.R. Sutton and G.J. Flynn, Proc. Lunar Planet. Sci. Conf., 18th (1988) 607.

[17] R. Bockman, M. Repo, R. Warrell, J.G. Pounds, W.M. Kwiatek, G.J. Long, G. Schidlovsky and K.W. Jones, in: X-Ray Microscopy II, eds., D. Sayre, M. Howells, J. Kirz and H. Rarback (Springer-Verlag, Berlin-Heidelberg-New York-London-Tokyo, 1988).

[18] K.W. Jones, B.M. Gordon, A.L. Hanson, W.M. Kwiatek and J.G. Pounds, Ultramicroscopy 24 (1988) 313.

[19] P. Spanne and M.L. Rivers, BioScience Abs. 1 (1988).

[20] A. Iida, K. Sakurai, Y. Gohshi and S. Komiya, Jpn. J. Appl. Phys. 27 (1988) L1825.

[21] A. Iida, A. Yoshinaga, K. Sakurai and Y. Gohshi, Anal. Chem. 58 (1986) 394.

[22] F.v. Langevelde, W.J.M. Lenglet, R.M.W. Overwater, R.D. Vis, A. Huizing, M.P.A. Viegers, C.P.G.M. Zegers and J.A. v.d. Heide, Nucl. Instr. Meth. A257 (1987) 436.

[23] A.C. Thompson, J.H. Underwood, Y. Wu, R.D. Giauque, K.W. Jones and M.L. Rivers, Nucl. Instr. Meth. A266 (1988) 318.

[24] Y. Gohshi, S. Aoki, A. Iida, S. Hayakawa, H. Yamaji and K. Sakurai, Jpn. J. Appl. Phys. 26 1987) L1260.

[25] B.M. Gordon and K.W. Jones, Nucl. Instr. Meth. B10/11 (1985) 293.

[26] K.W. Jones, P.A. Takacs, J.B. Hastings, J.M. Casstevens and C.D. Pionke, SPIE 749 (1987) 37.

[27] V.E. Baryshev, A.E. Gilbert, O.A. Kozmenko, G.N. Kulipanov and K.V. Zolotarev, Nucl, Instr. Meth. A261 (1987) 272.

[28] M.L. Rivers and S.R. Sutton, EOS, Trans. Am. Geophys. U. 7 (1989) 492.

[29] N.M. Halden, F.C. Hawthorne, J.J.G. Durocher and J.S.C. McKee, GAC/MAC, Program with Abstracts 14 (1989) A68.

[30] J.R. Chen, E.C.T. Chao, J.A. Minkin, J.M. Back, to be published.

[31] E.C.T. Chao, J.A. Minkin, J.M. Back, R.L. Erickson, L.J. Drew, P.M. Okita, E.H. McKee, J.E. Conrad, B. Turrin, M. Tatsumoto, W. Junwen, C.A. Edwards and R.V. Buden, Intl. Geol. Cong., Washington, D.C. (1989).

[32] Y. Suzuki, K. Usami, K. Sakamoto, H. Kozaka, T. Hirano, H. Shiono and H. Kohno, Jpn. J. Appl. Phys. 27 (1988) L461.

[33] B.P. Flannery, H.W. Deckman, W.G. Roberge and K.L. D'Amico, Science 237 (1987) 1439.

[34] J.R. Chen, B.M. Gordon, A.L. Hanson, K.W. Jones, H.W. Kraner, E.C.T. Chao and J.A. Minkin, Scanning Electron Microsc. 4 (1984) 1485.

[35] K. Sakurai, A. Iida and Y. Gohshi, Jpn. J. Appl. Phys. 26 (1987) 1937.

[36] G.E. Brown, G. Calas, G.A. Waychunas and J. Petiau, Rev. Mineral. 18 (1988) 431.

[37] G.A. Waychunas, G.E. Brown, C.W. Ponader and W.E. Jackson, Nature 332 (1988) 251.

[38] G.P. Huffman, F.E. Huggins, S. Mitra, N. Shah, R.J. Pugmire, B. Davis, F.W. Lytle and R.B. Greegor, Energy and Fuels, in press.

[39] C.J. Sparks and G.E. Ice, Mat. Res. Soc. Symp. Proc. 143 (1989) 223.

[40] R.D. Vis, in: Application of Synchrotron Radiation in Chemistry, eds., Catlow and Greeves (1989).

[41] K. Kim, in: X-Ray Data Booklet, LBL Pub. 490 (1985) 4-1.

[42] K.W. Jones and B.M. Gordon, Anal. Chem. 61 (1989) 341A.

[43] M. Ando and S. Aoki, preprint (1989).

[44] T. Hirano, S. Eguchi and K. Usami, Jpn. J. Appl. Phys. 28 (1989) 135.

[45] I. Brissaud, J.X. Wang and P. Chevallier, submitted to J. Radioanal. Nucl. Chem. (1989).

Table 1. SXRF microprobes

Ring	E_γ (keV)	Beam optics	Spatial resolution (μm)	MDL (ppm)	Field	Objects	Main elements	Comments	Reference
DORIS Hamburg FRG	white	collimator	50	1.5	Atmospheric Science, Geology	Aerosols, liquid inclusions	Fe,Zn		8
	white	mirror/collimator	3			Ni grains	Ni	line scanning technique	9
VEPP-3 Novosibirsk USSR	white	collimator	30		Geology	Rock samples		wiggler beam	10
	8-35	flat pyrolytic graphite/collimator	60	10			Fe to Sr		
		curved pyrolytic graphite/collimator	10	1					
SRS Daresbury UK	20	toroidal Si(111) /collimator	200 H 380 V 10's	10's		Organic matrix	Zn	wiggler beam X10 with HBL	22
NSLS Brookhaven USA	white	collimator	30	0.8-3	Geology	Carlin ores Sulfide minerals in coals	Au,Zn,Ga,As,Rb,Sr Ni,Cu, Zn, Se, As Mo,Tl,Pb		11,12 13
					Silicate melts		Mn,Fe,Zn,Y,Zr,Nb		14
				5-15	Cosmochemistry	Iron meteorites	Fe,Cu,Ni,Se,Ga,Ge		15
				30-300	Interplanetary dust particles		Cr,Mn,Fe,Ni, Cu Zn,Ga,Ge,Se,Br	7-25μm particle sizes	16
				1	Biomedical	Rat bones	Ga		17
				0.15 Fe to 4.2 Cd	Biology	Rat cerebellum	K,Ca,Mn,Fe,Cu, Zn,Hg,Se		18
			10 V 17 H			Tibia, ant head	Ca	Microtomography	19
	10	Multilayer spherical mirrors	10	1-40	Biology Geology	Algae, rat tissue Fluid inclusions in quartz	Fe,Zn,Cu,Ni Ca,Cl		4,23
	3-17	Si channel-cut monochromator/ellipsoidal mirror/collimator	5-30	.01-1					25
Photon Factory Tsukuba Japan	12.6	Flat Si(111)/collimator /reflector	<40 H 3mm V	2×10^{12} atoms/cm²	Material Science	Contamination layer of InP substrate	As,Ga	Grazing incidence technique	20
				<.001 (in soln.)		Aqueous soln. of metal ions	Zn,Mn,Ca		21
	7-20	Si(111)/collimator				Ceramic	Y	Microtomography 10μm resolution	44
	up to 10	Two Wolter type 1 optical systems	<10 V 30 H			Granite	Fe,Ca		24
DCI Orsay France			10						45

Figure captions

Figure 1. Brilliance of various synchrotron sources as a function of energy. APS (7 GeV, 100 mA). NSLS (2.5 GeV, 500 mA). Conventional x-ray tube data after Kim [41].

Figure 2. Schematic of the electron's motion in an insertion device with alternating magnetic field.

Figure 3. SXRF experimental arrangement used at the Photon Factory. 45° Incidence (solid line). IC: ionization chamber. After Iida et al. [20].

Figure 4. Various designs used to focus synchrotron radiation. a) SRS toroidal Si(111) crystal focuses and monochromatizes the beam. b) LBL microprobe uses two spherical multilayer mirrors in Kirkpatrick-Baez configuration. Beam is focused and monochromatized. c) Photon Factory Wolter type 1 optics focuses the beam. d) NSLS ellipsoidal mirror focuses the beam. Separate Si channel-cut monochromator is used. After Jones and Gordon [42] and Ando and Aoki [43].

Figure 5. SXRF multielement K line spectrum of aeschynite mineral grain from Bayan Obo ore deposit.

Figure 6. Computed tomogram of an ant head. Slice thickness 10μm. Image matrix 211 x 211. Pixel size 17 x 17μm^2. White beam filtered with 200μm Zn. After Spanne and Rivers [19].

Figure 7. Schematic of x-ray absorption cross section showing XANES and EXAFS regions. After Chen et al. [34].

Figure 8. Absorption spectra of Co metal and oxides using fluorescence detection. a indicates electron transitions from the 1s to the 3d-4s-4p admixed empty states. b indicates absorption into the pure 4p band. Since the interatomic distance is increased by compound formation, the 4p band becomes narrower and no longer admixes with the 3d band in oxides. After Sakurai et al. [35].

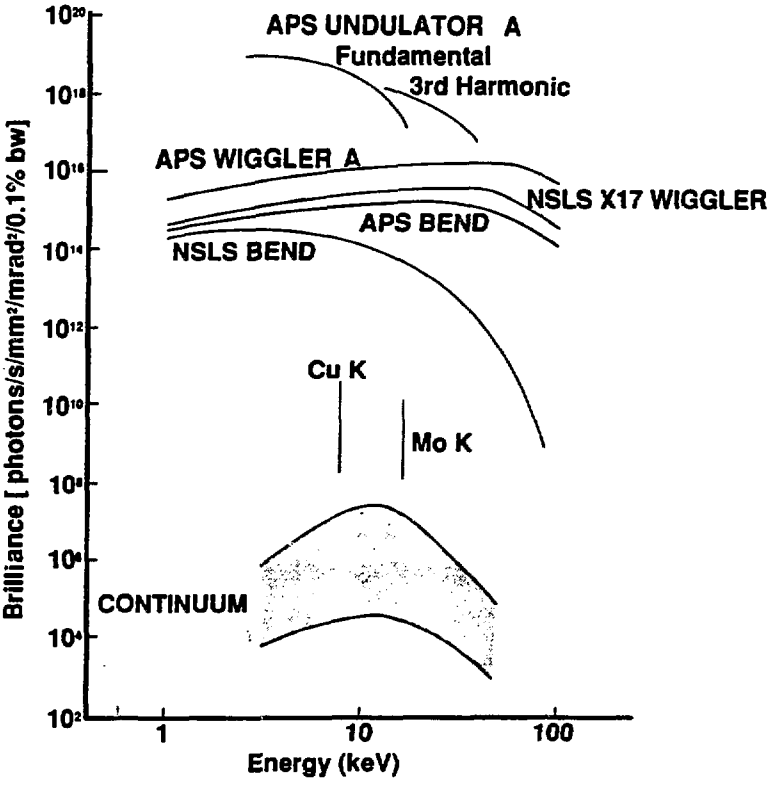
APS UNDULATOR A
Fundamental
3rd Harmonic
APS WIGGLER A
NSLS X17 WIGGLER
APS BEND
NSLS BEND
Cu K
Mo K
CONTINUUM
Brilliance [photons/s/mm²/mrad²/0.1% bw]
Energy (keV)
10²⁰
10¹⁸
10¹⁶
10¹⁴
10¹²
10¹⁰
10⁸
10⁶
10⁴
10²
1
10
100

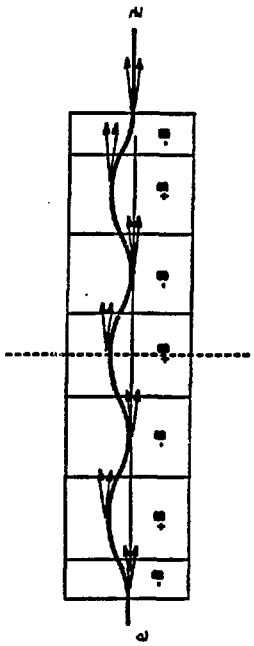

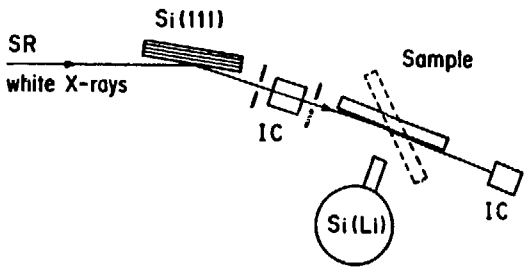
Si(111)
SR
white X-rays
Sample
IC
Si(Li)
IC

A.

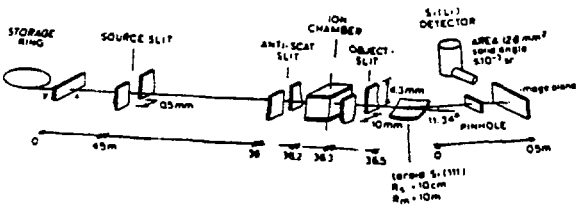
STORAGE RING
SOURCE SLIT
ION CHAMBER
ANTI-SCAT SLIT
OBJECT SLIT
DETECTOR
PINHOLE

B.

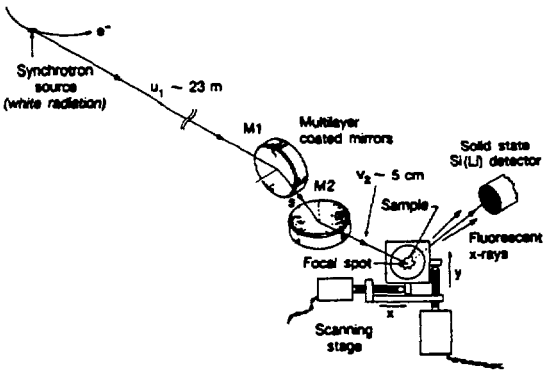
Synchrotron source (white radiation)
$u_1 \sim 23$ m
M1
Multilayer coated mirrors
M2
$v_2 \sim 5$ cm
Solid state Si(Li) detector
Sample
Fluorescent x-rays
Focal spot
Scanning stage

C.

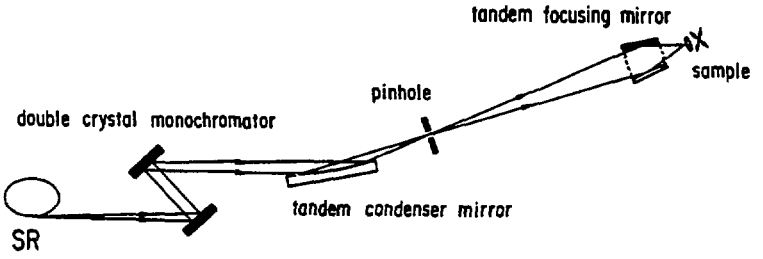
tandem focusing mirror
sample
pinhole
double crystal monochromator
tandem condenser mirror
SR

D.

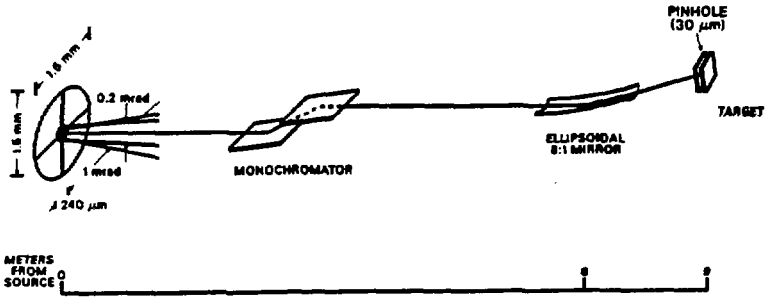
PINHOLE (30 μm)
TARGET
ELLIPSOIDAL 8:1 MIRROR
MONOCHROMATOR
0.2 mrad
1 mrad
METERS FROM SOURCE

Aeschynite in Bayan Obo sample 8 B38 - 1 SXRF File: SUNY 4.42

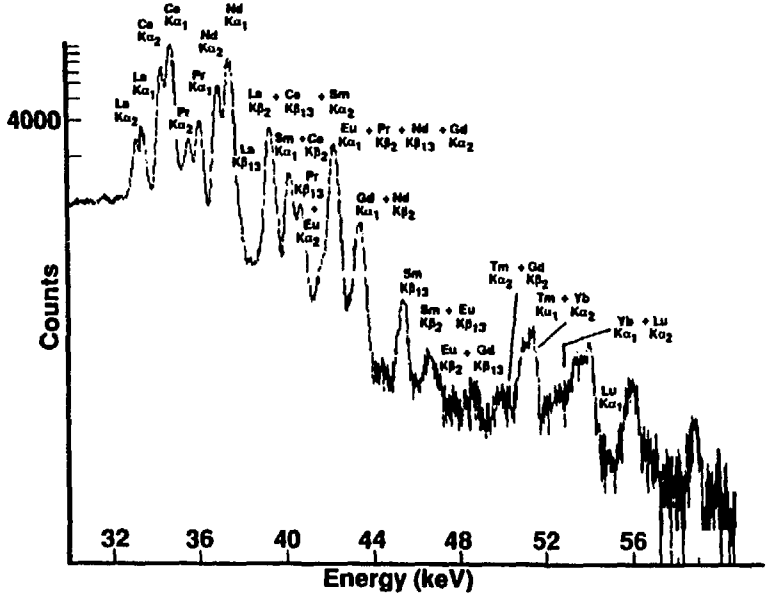

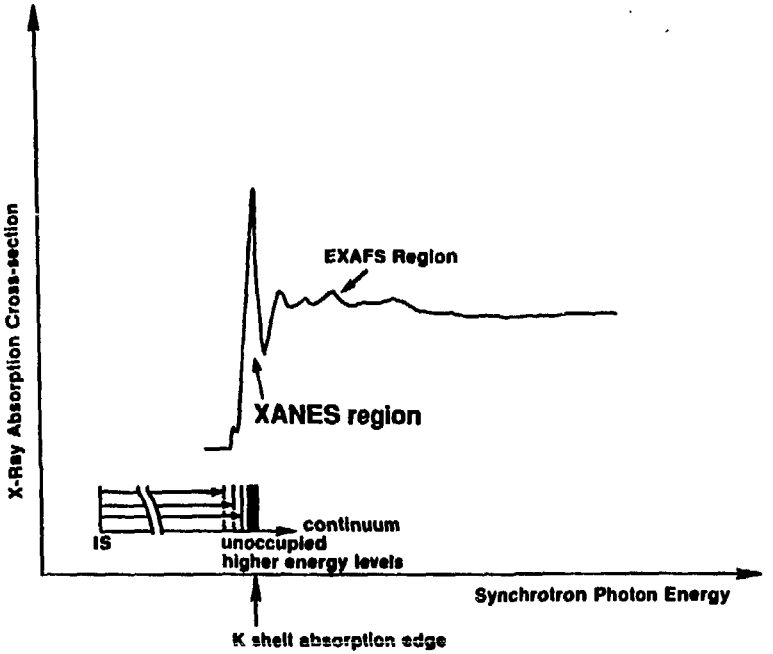
X-Ray Absorption Cross-section
EXAFS Region
XANES region
IS
continuum
unoccupied
higher energy levels
Synchrotron Photon Energy
K shell absorption edge

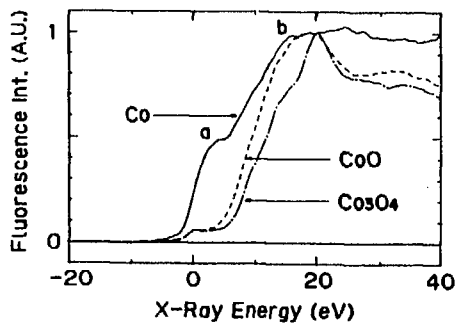
Fluorescence Int. (A.U.)
1
0
-20
0
20
40
X-Ray Energy (eV)
Co
a
b
CoO
Co3O4